Journal of Theoretical and Applied Information Technology
31st March 2013. Vol. 49 No.3

ISSN: 1992-8645 www.jatit.org E-ISSN: 1817-3195

RESEARCH ON WHEELBASE, WHEELBASE DIFFERENCE AND WHEEL STATIC RADIUS DETECTION BASED ON STEREO VISION

[1]CHEN XU, [2]LIN GUOYU

[1] School of Information & Control, Nanjing University of Information Science & Technology, China,

[2] School of Instrument Science and Engineering, SouthEast University, China

E-mail: [1]Sonia.chen@163.com, [2]Andrew.Lin@seu.edu.com

ABSTRACT

A stereo vision method is presented to measure wheelbase, wheelbase difference and wheel static radius, and the key is to locate the wheel center. The aluminum alloy wheel hub is the research subject in the method, and its contour is extracted and fitted as an ellipse curve. To improve the matching precision, a new un-tangent constraint is adopted based on which stereo matching is carried out. Then a spatial circle projection algorithm with low time complexity and high accuracy is proposed to reconstruct 3D coordinates of wheel center. After that, the measurement models of wheelbase, wheelbase difference and wheel static radius is described in details. At last experiments are performed to verify our proposed method. In experiments, wheelbase, wheelbase difference and wheel static radius of three different cars are measured, and then the results are compared to manual measurement results. Experiments have proved that the proposed method could acquire the wheelbase, wheelbase difference and wheel static radius fast and accurately.

Keywords: *Wheelbase Difference, Static Radius, Wheel Center, Stereo Vision, 3D Reconstruction*

1. INTRODUCTION

The vehicle wheelbase, wheelbase difference and wheel static radius are three important vehicle dimension parameters, and they have direct influence on vehicle performance. The wheel static radius is the distance from wheel center to the vehicle support plane and it plays an important role in braking moment calculation and performance analysis. The wheelbase is the distance between two wheel centers on the same side as Figure 1 (a) shows, where A_L is the left wheelbase and A_R is the right wheelbase. The wheelbase is for the research of braking performance, maneuverability and ride comfort. The difference between A_L and A_R is vehicle wheelbase difference, which is expressed by $\Delta A_d = A_L - A_R$ shown in Figure 1 (a) and it has a significant influence on automotive performance. Due to the automotive frame and bridge distortion, abrasion of axial connection parts, the front axle of vehicle is usually not parallel to the rear axle, and then the difference ΔA_d appeared. When the difference ΔA_d exceeds a certain limit, vehicles stability changed for the worse; when braking or running at high speed, it will enable the automobile occur to turn to radical sliding or overturn; when straight line travel, it will increase the body's road width, impact on road safety, increase tire wear, bring economic losses and potentially dangerous [1]-[3]. Therefore, it is necessary to detect the wheelbase difference regularly to ensure the vehicles in good working status.

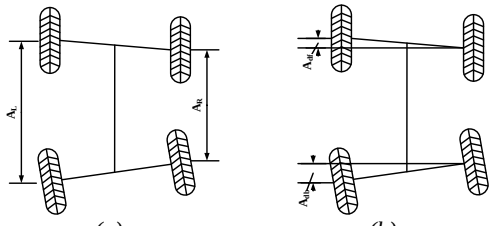

(a) *(b)*

Figure 1 :Diagram of Wheelbase Difference Model (a) Absolute Measurement Model, (b) Relative Measurement Model

1.1 Related Work

Traditionally the vehicle dimension is measured by artificial methods, and it has many drawbacks including inefficiency and worse repeatability. Till now some automatic measurement methods have been presented [4]-[7]. In Ref. [4] a method integrated with photoelectric switches, cameras and radar is presented to measure the vehicle height, length and width. In Ref. [5] a stereo vision method

ISSN: 1992-8645 www.jatit.org E-ISSN: 1817-3195

with laser projection is introduced to acquire the vehicle tread. And in Ref. [6] and [7] a vehicle dimensional parameters measuring system based on visual stereo equipped with monocular camera and stereo camera is described, however the experiments are not sufficient to support this method. However there is no system or method proposed to measure the three vehicle dimension parameters we concerned simultaneously. Several researchers raised the algorithm based on vision to measure the radius, and more researchers focus on the detection of wheelbase and wheelbase difference [8]-[15]. At present the detection of wheelbase and wheelbase difference are divided into two types: absolute measurement and relative measurement. Absolute measurement means wheelbase difference is measured directly according to its definition as shown in Figure 1 (a). By measuring the wheel's projection on the ground with steel tape, vehicle wheelbase and wheelbase difference can be calculated [8]. With the development of detection technology, methods with laser, photosensitive sensor et al. has been proposed [9][10]. Shengquan Jia added laser ranger finder to the four automobile wheel aligner instruments, which could accurately measure wheelbase and wheelbase difference in a few seconds [9]. Hongmei Shang described a vehicle wheelbase difference detection method based on stereo vision which extract the wheel center in image and then calculate the wheel hub center's 3D coordinates by means of stereo matching and 3D reconstruction algorithm [10]. The relative measurement model does not measure the wheelbase directly like absolute measurement model. According to the geometric principle of relative measurement shown in Figure 1 (b), wheelbase difference can be expressed by $\Delta A_d = \Delta A_{df} + \Delta A_{db}$, where ΔA_{db} is the deflection of rear wheel and ΔA_{df} of front wheel. ΔA_{df} and ΔA_{db} could be acquired by laser method, piezoelectric method, or vision method etc. [11]-[15]. Hongda PAN and other researchers put forward mounting a camera under ground and capture the tire images when the vehicle passing by. Through edge extraction of tire image, calculating the center position of vehicle axle and measurement of the difference between the front and rear axle, the vehicle wheelbase difference can be acquired [11]. Libin Zhang etc. proposed a new detecting method of wheelbase difference based on piezoelectric tire print [12]-[15].

In the paper, we propose a measurement method based on stereo vision, which has the following characteristics: 1) The non-contact measurement method based on stereo vision can obtain the wheelbase, wheelbase difference and static wheel radius simultaneously. 2) The wheel center coordinate is calculated by stereo matching and the perspective projection model of the spatial circle. This method has the advantage of high accuracy and low computational complexity. 3) The wheel center is acquired via the measurement of the wheel hub center, which contributes to the improvement of reliability and robustness. And the experiments have proved that the method has the good characteristic of repeatability, stability and accurate precision.

1.2 An Overview of Our Approach

In the measurement system, BMU (Basic Measurement Unit) is a basic measurement module based on stereo vision, which detects the wheel center and calculates its 3D coordinates. As is shown in Figure 2, BMU_L1 is composed of Camera C1 and Camera C2; BMU_L2 of Camera C3 and Camera C4; BMU_R1 of Camera C5 and Camera C6; BMU_R2 of Camera C7 and Camera C8. BMU_L1, BMU_L2, BMU_R1 and BMU_R2 detect and reconstruct the wheel center of left front wheel, left back wheel, right front wheel and right back wheel respectively. The four BMUs should be calibrated by 3D target beforehand to obtain the extrinsic parameter matrixes among them and the equation of the vehicle supporting plane. When 3D coordinates of the four wheel centers are obtained, the wheelbase, the wheelbase difference and static wheel radius can be figured out according to the corresponding mathematical model.

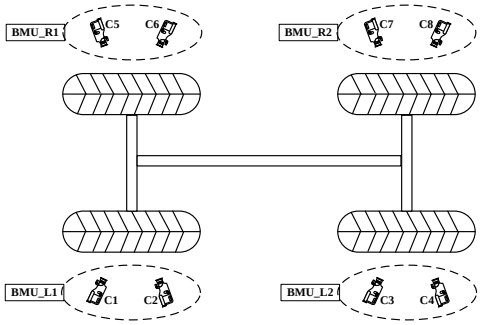

Figure 2 : Diagram of Measurement System

1.3 Outline of the Paper

The remainder of the paper is organized as follows: Section 2 describes a wheel hub of 3D image reconstruction algorithm, which allows the extraction of the hub center coordinate more accurately. Section 3 is dedicated to the description of measurement method for wheelbase, wheelbase difference and static wheel radius. In Section 4, we explain the extensive experimental studies

ISSN: 1992-8645 www.jatit.org E-ISSN: 1817-3195

conducted and demonstrate the results. At last we conclude this work in Section 5.

2. MEASUREMENT METHOD FOR WHEEL HUB CENTER

2.1 Characteristics Extraction for Ellipse

Most relevant literature on robust ellipse fitting is proposed [16]-[18] and good result is achieved. Generally they use a least-squares method and remove outliers after fitting. In the paper, this method is also exploited to extract the ellipse characteristics of wheel hub. However, due to complex background and noise, there may be false ellipse characteristics been extracted. So priori information of wheel is used. For most wheels, the aluminum alloy wheel hub is light and the tire is black, so it is a good cue to obtain the correct ellipse. Firstly the binary image is obtained through OSTU threshold segmentation method in the area near the fitting ellipse. Then two discriminate conditions for wheel hub is proposed here: ① In the binary image, the gray values of most pixels in interior of the fitting ellipse are 255 due to light wheel hub. ② In the binary image, the gray values of most pixels in exterior of the fitting ellipse are 0 due to black tire.

2.2 Ellipse Stereo Matching with Un-tangent Constraint

After obtaining the ellipse characteristics of wheel hub in the stereo images, 3D coordinates of every point in wheel hub contour can be calculated by stereo matching and 3D reconstruction. The traditional ellipse stereo matching is based on epipolar line constraint and sequence constraint which means sequence of two points in the right epipolar line shall be the same in the left epipolar line. It is notable that good matching result can be acquired with these two constraints except the area where the epipolar line and the fitting ellipse are tangent approximately, shown in Figure 3.

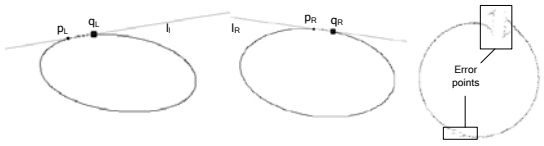

(a) (b) (c)

Figure 3 : Epipolar Line and Fitting Ellipse are Tangent Approximately
(a) Epipolar Line in Left Image, (b) Epipolar Line in Right Image, (c) 3D Reconstruction Result Projected to Circle Plane

In Figure 3, l_L, l_R are epipolar line in left image and right image respectively, p_L, q_L are the intersection points of epipolar line l_L and fitting ellipse in left image, and p_R, q_R are the intersection points of epipolar line l_R and fitting ellipse in right image. According to the epipolar line constraint and sequence constraint, p_R and q_R is the correct correspondence of p_L and q_L respectively. However after a large number of experiments, we find that because of the existence of epipolar line calculation error, ellipse curve fitting error and image process error, in the area where the epipolar line and the fitting ellipse being tangent approximately, although some correspondence satisfy the epipolar line constraint and sequence constraint, the reconstructed 3D points are obvious wrong as shown in Figure 3 (c).

Aiming at the problem, a new constraint named un-tangent constraint for ellipse is proposed. The key is to keep away from error prone area where the epipolar line and the fitting ellipse being tangent approximately. The un-tangent constraint is composed of two sub-constraints:

Constraint 1: The distance between the intersection points of epipolar line and fitting ellipse should be greater than the predefined threshold T_E, which can be calculated as follow:

$$T_E = \begin{cases} M_L / 5 & |\theta_L - \theta_E| < |\theta_L - \theta_E| \\ M_S / 5 & |\theta_S - \theta_E| \geq |\theta_S - \theta_E| \end{cases} \quad (1)$$

Where θ_L and θ_S are angles of major axis and minor axis respectively, θ_E is the angle of current epipolar line, M_L and M_S are the length of major axis and the length of minor axis of the fitting ellipse in image separately. The Equation (1) expresses that the threshold T_E is calculated according to the length of major axis when current epipolar line is close to the direction of major axis, otherwise according to the length of minor axis.

Constraint 2： As Figure 4 shown, the ellipse curve is divided into two parts by epipolar line l_t. Then the maximal distance from points in each ellipse part to epipolar l_t is calculated and denoted by d1 and d2. Here suppose d1≤d2, then d1/d2 should be greater than T_d where is set to 0.05 in our experiments.

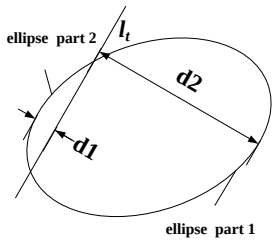

Figure 4 : Diagram of Constrain 2

ISSN: 1992-8645 www.jatit.org E-ISSN: 1817-3195

According to the constraint, the stereo matching process is constructed as follows:

(1) Compute the intersection points between the corresponding left epipolar line and ellipse. Here p_{Li} and q_{Li} are intersection points in the left image, p_{Ri} and q_{Ri} are intersection points in the right image.

(2) Calculate the distance between p_{Li} and q_{Li}, and select two points with maximum distance in the left epipolar line of the left image, denoted by p_{Lk} and q_{Lk}, the same to the p_{Ri} and q_{Ri} in right image, denoted by p_{Rk} and q_{Rk}.

(3) According to the epipolar line constraint and sequence constraint only, the corresponding points of p_{Lk}, q_{Lk}, p_{Rk} and q_{Rk} are calculated respectively, denoted by p'_{Lk}, q'_{Lk}, p'_{Rk} and p'_{Lk}.

(4) Based on the four correspondence (p_{Lk}, p'_{Lk}), (q_{Lk}, q'_{Lk}), (p_{Rk}, p'_{Rk}) and (q_{Rk}, q'_{Rk}), the correspondence of other points in ellipse are established with epipolar line constraint, sequence constraint, continuity constraint and un-tangent constraint.

2.3 High-precision Positioning Algorithm for Wheel Center

Through the stereo matching method mentioned above, 3D coordinates of all the points on the wheel hub contour can be obtained, denoted by $P_{1i}=[X_{1i}, Y_{1i}, Z_{1i}]^T$. Here an effective algorithm based on 2D plane projection is used to gets the wheel canter's 3D coordinates. The following is the adopted algorithm is details:

(1) Since the wheel hub contour is located in a spatial plane L_0 which is expressed by the equation: AX+BY+CZ+1=0, the points $P_{1i}=[X_{1i}, Y_{1i}, Z_{1i}]^T$ are lied in plane L_0 too. Bringing the points $P_{1i}=[X_{1i}, Y_{1i}, Z_{1i}]^T$ into the plane equation may obtain over determined equations, which will be solved by SVD to get the parameters [A, B, C, 1] of plane L_0.

(2) The points $P_{1i}=[X_{1i}, Y_{1i}, Z_{1i}]^T$ are projected to the spatial plane L_0 and the projection points denoted as $P_{2i}=[X_{2i}, Y_{2i}, Z_{2i}]^T$ are generated. According to the theory of analytic geometry, the vector connecting point P_{1i} to P_{2i} should parallel to the vertical vector of the spatial plane L_0, which can be expressed as follows:

$$X_{2i} = X_{1i} + At \qquad Y_{2i} = Y_{1i} + Bt \qquad Z_{2i} = Z_{1i} + C \tag{2}$$

Where, t is parameter of parametric equation of line. Furthermore P_{2i} is on the spatial plane L_0, so it satisfies the plane equation $AX_{2i}+BY_{2i}+CZ_{2i}+1=0$. Then the parameter t can be solved:

$$t = -\frac{AX_{1i} + BY_{1i} + CZ_{1i} + 1}{A^2 + B^2 + C^2} \tag{3}$$

So, by inputting the parameter t into Equation (3), the 3D coordinates of P_{2i} can be calculated.

(3) Supposing that $p_t=[X_0, Y_0, Z_0]^T$ is a point in the spatial plane L_0, according to the Space Geometry Principle there exists a spatial plane L_1 which is perpendicular to the spatial plane L_0 and passes through the point p_t. The vector of the spatial plane L_1 is expressed as $[A_1, B_1, C_1, D_1]$, where $A_1=-A$, $B_1=2B$, $C_1=(A_2-2B_2)/C$, $D_1=AX_0-2BY_0-(A^2-2B^2)Z_0/C$.

(4) Likewise, there exists one spatial plane L_2 which is perpendicular to the spatial plane L_0 and L_1 and passes through the point p_t too. The parameter of the spatial plane L_1 is denoted as $[A_2, B_2, C_2, D_2]$, where $A_2=BC_1-CB_1$, $B_2=CA_1-AC_1$, $C_2=AB_1-BA_1$, $D_2=-((BC_1-CB_1)X_0+(CA_1-AC_1)Y_0+AB_1-BA_1)Z_0]$.

(5) A new coordinate systems O'X'Y'Z' is constructed, where the origin of O'X'Y'Z' is the point p_t, and O'X'Y' plane, O'X'Z' plane and O'Y'Z' plane is spatial plane L_0, L_1 and L_2 respectively.

(6) The projection points $P_{2i}=[X_{2i}, Y_{2i}, Z_{2i}]^T$ is converted to the points P_{3i} in O'X'Y'Z'. Because the points P_{2i} lies in spatial plane L_0 which is O'X'Z' plane also, Z coordinates of points P_{3i} is 0, Y coordinate and X coordinate of points P_{3i} is the distance from the point P_{2i} to the O'X'Z' plane, and O'Y'Z' plane respectively. Equation (4) shows the calculation.

$$x_i' = \frac{A_2X_{2i} + B_2Y_{2i} + C_2Z_{2i} + D_2}{\sqrt{A_2^2 + B_2^2 + C_2^2}}$$
$$y_i' = \frac{A_1X_{2i} + B_1Y_{2i} + C_1Z_{2i} + D_1}{\sqrt{A_1^2 + B_1^2 + C_1^2}}$$
$$z_i' = 0 \tag{4}$$

(7) The curves composed of projection point P_{3i} are fitted by ellipse fitting method in O'X'Z', then the 2D coordinates of fitting ellipse center in the O'X'Z' can be calculated, denoted by $O_c' = [x_c', y_c']^T$.

(8) Convert 2D coordinates of the fitting ellipse center O_c' in O'X'Z' to 3D coordinates $[X_C, Y_C, Z_C]^T$ in OXYZ. For $n_1=[A_2, B_2, C_2]^T$, $n_2=[A_1, B_1, C_1]^T$ and $n_3=[A, B, C]^T$ are the normal vector of

Journal of Theoretical and Applied Information Technology
31st March 2013. Vol. 49 No.3

ISSN: 1992-8645 www.jatit.org E-ISSN: 1817-3195

O'Y'Z' plane, O'X'Z' plane and O'X'Y' plane respectively, we can acquire the basic vectors of them which is denoted as $[A'_2, B'_2, C'_2]^T$, $[A'_1, B'_1, C'_1]^T$ and $[A', B', C']^T$.

Then the 3D coordinates of O_c can be obtained by Equation (5):

$$\begin{aligned} X_C &= A'_2 x_c + A'_1 y_c + X_0 \\ Y_C &= B'_2 x_c + B'_1 y_c + Y_0 \\ Z_C &= C'_2 x_c + C'_1 y_c + Z_0 \end{aligned} \quad (5)$$

Here, $[X_C, Y_C, Z_C]^T$ is the 3D coordinates of wheel hub center O_c.

According to the eight steps mentioned above, 3D coordinates of the wheel hub center O_c can be acquired. It is noteworthy that due to the fitting error and the 3D reconstruction error, the reconstructed spatial circle is not a standard circle but an ellipse whose major axis is very close to minor axis. So in step (7) the ellipse fitting method is exploited.

3 EXPERIMENTS AND ANALYZATION

Experiments are performed on real vehicle to demonstrate the utility of the proposed algorithm. Three different cars including Roewe 550, Nissan Teana and Buick Lacrosse are used as experimental object to verify the validity of the proposed method in practice. The vision sensors used in the real car measuring experiment are Canon A75 digital camera with 3 mega pixels and 2048×1536 resolution. In the following experiments 8 Canon A75 digital cameras are used and 4 BMUs are constructed.

3.1 Manual measurement

The manual measurement with tape is used for comparison, and the average measurement is shown in Table 1. In Table 1, J_{JLk}(k=1-4) is the left front, right front, left rear and right rear wheel radius respectively, J_{WB1} and J_{WB2} is the left wheelbase and right wheelbase separately, and J_{WBD} is the difference of left wheelbase J_{WB1} and right wheelbase J_{WB2}.

Table 1 : Results Measured Manually (unit: mm).

	J_{JL1}	J_{JL2}	J_{JL3}	J_{JL4}	J_{WB1}	J_{WB2}	J_{WBD}
Roewe 550S	288	289	308	305	2702	2711	-9
Nissan Teana	309	313	329	331	2776	2781	-5
Buick Lacrosse	314	318	335	333	2839	2835	4

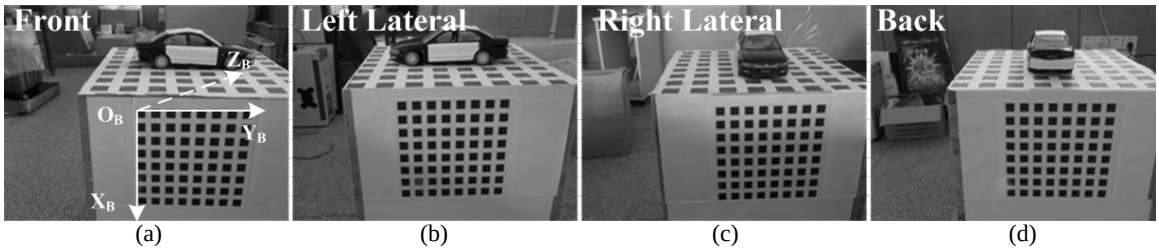

(a) (b) (c) (d)

Figure 5 : Calibration Target from 4 Views
(a) Front Side, (b) Lleft Lateral Side, (c) Right Lateral Side, (d) Back Side

3.2 Global Calibration

In order to transform the measurement data acquired from the 4 BMUs into a global coordinate system, global calibration is needed. Figure 5 shows the calibration target used in the experiment. The target coordinate $O_BX_BY_BZ_B$ is set up in front side. In $O_BX_BY_BZ_B$ the origin O_B is the top left corner of the top left square, X_B axis and Y_B axis parallel to the sides of the squares respectively, and X_Z axis is perpendicular to the front plane.

A calibration target can not appear in all field views of the 4 BMUs due to long wheelbase, so a calibration structure shown in Figure 6 is designed to solve the problem, in which the target coordinate $O_BX_BY_BZ_B$ of BMU_L1 is selected as the global coordinate $O_WX_WY_WZ_W$.

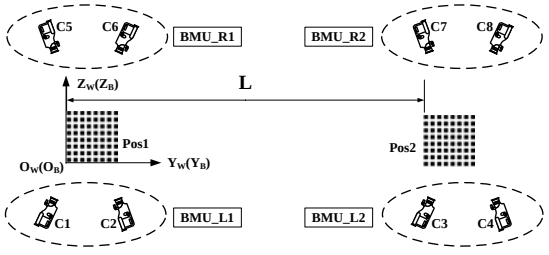

Figure 6 : Diagram of Calibration Structur.

The detailed calibration procedure is as follows:

(1) The calibration target is placed at the position Pos1 to make the front chessboard in the FOV of BMU_L1 and the back chessboard in the FOV of BMU_R1. Then the transformation matrix from the target coordinate of BMU_R1 to that of BMU_L1

Journal of Theoretical and Applied Information Technology
31st March 2013. Vol. 49 No.3

ISSN: 1992-8645 www.jatit.org E-ISSN: 1817-3195

is calculated, denoted as [R_{L1R1} T_{L1R1}] and shown as Equation (6);

$$R_{L1R1}=\begin{bmatrix}1&0&0\\0&-1&0\\0&0&1\end{bmatrix}\quad T_{L1R1}=\begin{bmatrix}0&190&400\end{bmatrix} \tag{6}$$

(2) The calibration target is moved to the position Pos2 along O_WY_W direction to make the front chessboard in the FOV of BMU_L2 and the back chessboard in the FOV of BMU_R2. The distance from Pos1 to Pos2 is L. Then the transformation matrix from the target coordinate of BMU_L2 to that of BMU_L1 is calculated, denoted as [R_{L1L2} T_{L1L2}] and shown as Equation (7) ;

$$R_{L1L2}=\begin{bmatrix}1&0&0\\0&1&0\\0&0&1\end{bmatrix}\quad T_{L1L2}=\begin{bmatrix}0&L&0\end{bmatrix} \tag{7}$$

(3) Similar to the geometric relation between BMU_R1 and BMU_L1, the transformation matrix from the target coordinate of BMU_R2 to that of BMU_L2 can be acquired. Then on the basis of the geometric relation between BMU_L1 and BMU_L2, the transformation matrix from the target coordinate of BMU_R2 to that of BMU_L1 is calculated, denoted as [R_{L1R2} T_{L1R2}] and shown as Equation (8) ;

$$R_{L1R2}=\begin{bmatrix}1&0&0\\0&-1&0\\0&0&1\end{bmatrix}\quad T_{L1R2}=\begin{bmatrix}0&190+L&400\end{bmatrix} \tag{8}$$

After completing the global calibration, according to the constraint which is that the vehicle supporting plane parallels to OWYWZW plane, the vehicle supporting plane equation X=H is got where H is the distance from the origin OW to the vehicle supporting plane and H can be measured in advance.

3.3 Measurement Experiment

After completing global calibration, we keep the four BMUs stationary, drive the car slowly and return wheels before stopping at the specified location. Figure 7 shows the part of the measurement scene, and Figure 8 shows the fitting ellipse of the wheel hub and the 3D reconstruction result of four wheel hub, and the dots mean the wheel centers.

During the experiment, the process including driving the vehicle to the specified region, measuring with proposed method and putting off performs 10 times. The mean absolute error (|Err|), mean square deviation (Var) and maximal absolute error (MaxErr) of measurement are calculated and shown in Table 2.

Figure 7 : Part of Measurement Scene

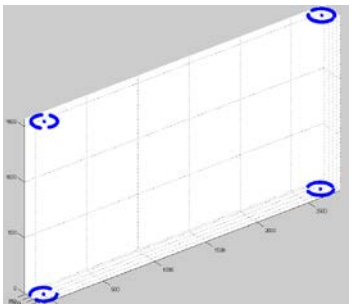

Figure 8 : 3D Reconstruction Result

Table 2 : |Err|, Var and MaxErr of the Experimental Results (unit: mm)

	Roewe 550S			Nissan Teana			Buick Lacrosse		
	|Err|	Var	MaxErr	|Err|	Var	MaxErr	|Err|	Var	MaxErr
J_{JL1}	1.34	0.13	2.00	1.24	0.20	1.90	0.82	0.15	1.30
J_{JL2}	1.21	0.13	1.70	1.44	0.22	2.00	1.30	0.17	1.90
J_{JL3}	1.10	0.12	1.80	1.90	0.14	2.40	1.25	0.26	1.90
J_{JL4}	1.13	0.17	1.90	1.51	0.26	2.20	1.10	0.22	1.80
J_{WB1}	2.11	0.28	2.90	3.00	0.11	3.60	2.77	0.26	3.70
J_{WB2}	3.35	0.26	4.10	2.84	0.39	3.50	3.48	0.21	4.20
J_{WBD}	1.24	0.26	2.30	0.6	0.41	1.20	0.87	0.51	1.70

The error can be considered as system error and compensation can be used to improve precision. To verify this, we recalculate the average absolute error by adding the average error to J_{WB1} and J_{WB2}, and give the result in Table 3. Figure 9 shows the errors of J_{WB1} and J_{WB2} for three vehicles with/without compensation. It can be seen that error compensation effectively reduces the error to below 1mm and makes the proposed method meets the requirement of the measurement precision.

ISSN: 1992-8645 www.jatit.org E-ISSN: 1817-3195

Moreover, it is clear that the error of J_{WBD} is large due to error superimposition of left wheelbase and right wheelbase. In general the method of averaging the result of several measurements can improve the measurement precision. However it still does not work indeed and the error is unacceptable. As mentioned earlier, the wheelbase compensation can effectively improve the wheelbase's measuring accuracy. So could it compensate the average J_{WBD}? The average J_{WBD} with/without wheelbase compensation is listed in Table 4, which shows that the error of average J_{WBD} is beyond 1mm without wheelbase compensation, and the error is almost zero after wheelbase compensation. It can be seen clearly that the measuring accuracy of J_{WBD} can be improved by wheelbase compensation.

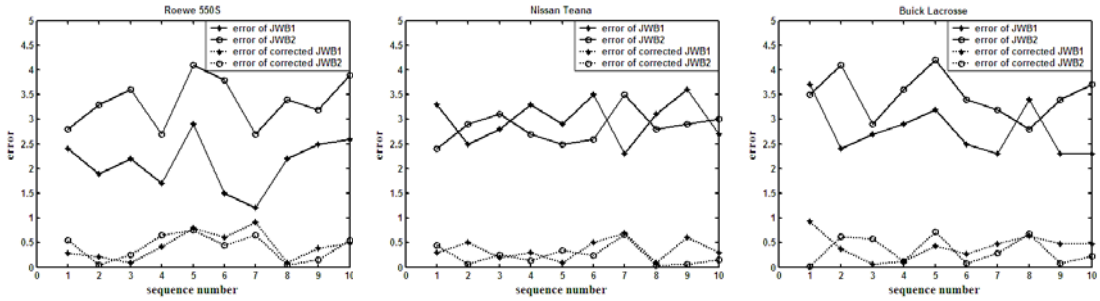

(a) *(b)* *(c)*

Figure 9 : Error Comparisons with/without Compensation for Chree Cars (a) Roewe 550S, (b) Nissian Teana, (c) Buick Lacrosse

Table 3 : Absolute Error after System Error Compensation (unit: mm)

Experiment index		1	2	3	4	5	6	7	8	9	10
Roewe 550S	J_{WB1}	0.29	0.21	0.09	0.41	0.79	0.61	0.91	0.09	0.39	0.49
	J_{WB2}	0.55	0.05	0.25	0.65	0.75	0.45	0.65	0.05	0.15	0.55
Nissan Teana	J_{WB1}	0.30	0.50	0.20	0.30	0.10	0.50	0.70	0.10	0.60	0.30
	J_{WB2}	0.44	0.06	0.26	0.14	0.34	0.24	0.66	0.04	0.06	0.16
Buick Lacrosse	J_{WB1}	0.93	0.37	0.07	0.13	0.43	0.27	0.47	0.63	0.47	0.47
	J_{WB2}	0.02	0.72	0.58	0.12	0.72	0.08	0.28	0.68	0.08	0.22

Table 4 : Wheelbase Difference with/without Wheelbase Compensation (unit: mm)

	without wheelbase compensation		with wheelbase compensation	
	Average J_{WBD}	J_{WBD} error	Average J_{WBD}	J_{WBD} error
Roewe 550S	-7.8	1.2	-8.9	0.1
Nissan Teana	-5.2	0.2	-5.0	0.0
Buick Lacrosse	4.7	0.7	3.9	0.1

4 CONCLUSIONS

In practical applications vehicle geometry dimension is traditionally measured manually. The method has the shortcoming of inefficiency and worse repeatability. With the development of science and technology, laser method, photosensitive method etc have been proposed. This paper presents a measurement method based on stereo vision, which is characterized by acquiring wheelbase, wheelbase difference and static wheel radius simultaneously. The key of the proposed method is the extraction and reconstruction of the wheel hub center, which could improve accuracy and reduce time complexity. In experiments both simulation data and real vehicle are used to demonstrate the utility of the proposed method, and then the source of error and its correction are analyzed. The experiment result verifies the validity and feasibility of the proposed method which can substitute for manual measurement and be a fast, simple and economical technique for vehicle dimension measurement.

ACKNOWLEDGEMENT

This work is supported by the National Natural Science Foundation of china (Grant No. 61272223).

ISSN: 1992-8645 www.jatit.org E-ISSN: 1817-3195

REFRENCES:

[1] Jianmin MA, "Study on the Brakeforce and Brake System of the Flame Proof Rubber Tyre Vehicle of Coal Mine", *Coal Technology*, Vol. 26, No. 4, 2007, pp. 11-14.

[2] Lee, J. H., and Yoo, W. S., "Predictive control of a vehicle trajectory using a coupled vector with vehicle velocity and sideslip angle", *International Journal of Automotive Technology*, Vol. 10, No. 2, 2009, pp. 211-217.

[3] Asi Osman, "Fatigue failure of a rear axle shaft of an automobile", *Engineering Fatigue Analysis*, Vol. 13, No. 8, 2006, pp. 1293-1302.

[4] Xiaoyun He, "Automaticsizing System in Size Parameters of Vehicle", *Modern Compute*, Vol. 6, 2011, pp. 34-36.

[5] Guoyu Lin, Wenhu Qin and Xu Chen, "The Measurement Method of Vehicle Wheel Track Based on Stereo", *Microcomputer Information*, Vol. 26, No. 9, 2010, pp. 15-17, 12.

[6] Xiaodong Bian, Weigong Zhang and Zhanjun Guo, "Vehicle Dimensional Parameters Measuring System Based on Visual Servoing", *Measurement & Control Technology*, Vol. 22, No. 5, 2003, pp. 40-42,47.

[7] Xiaodong Bian, Weigong Zhang and Zhanjun Guo, "Vehicle Dimensions Measurement Based on Vision Servoing Technology", *Automotive Engineering*, Vol. 26, No. 3, 2004, pp. 341-344.

[8] Yuehua Tian and Chunxu Liu, "Talk about the Quick-testing of the New Technology of Automobile Axle Base Difference between Left and Right", *Communications Standardization*, Vol. 6, No. 3, 2002, pp. 46-48.

[9] Shengquan Jia, Fei Tong, Dechao Song and etc., "Appliance of Laser Measurement in Measuring the Vehicle Wheelbase", *Electrical Automation*, Vol. 29, No. 3, 2009, pp. 66.

[10] Hongmei Shan, Jian Su, Li-bin Zhang and etc., "New method for wheelbase difference detection based on stereovision", *Journal o f Jilin University(Engineering and Technology Edition)*, Vol. 40, No. 3, 2010, pp. 645-649.

[11] Hongda Pan, Rong Chen, Jian Su and etc., "Research on detecting of the automobile wheelbase difference with image processing", *China Journal of Highway and Transport*, Vol. 16, No.2, 2003, pp. 119.

[12] Hongda PAN, Libin ZHANG, Zhengrui JIA and etc., "Fast measuring of axle distance difference based on monocular vision for ground mark recognition of vehicular wheel", *Journal of Chang'an University (Natural Science Edition)* , Vol. 29, No.5, 2009, pp. 107-111.

[13] Libin Zhang, Jian Su, Hongying Shan and etc., "Error compensation method of piezoelectric detection by tire print of vehicle wheelbase difference", *Journal of Jilin University (Engineering and Technology Edition)*, Vol. 41, No. 2, 2011, pp. 327-332.

[14] Libin Zhang, Lijun Chen, Yongjun Tian and etc., "Piezoelectric Detection Device and Experimental Analysis of Automobile Wheelbase Difference", *2010 2nd International Conference on Signal Processing Systems. Dalian, China*, 2010, pp. 407-410.

[15] Libin Zhang, Yongjun Tian, Hongying Shan and etc., "Study of detecting method of automobile wheelbase difference based on piezoelectric signal", *International Conference on Intelligent Computation Technology and Automation. Changsha*, China, 2010, pp. 414-420.

[16] Sung Joon Ahn, Wolfgang Rauh and Hans-Jürgen Warnecke, "Orthogonal distances fitting of implicit curves and surfaces", *IEEE trans. PAMI*, Vol. 24, 2002, pp. 620–638.

[17] Sung Joon Ahn, Wolfgang Rauh and Hans-Jürgen Warnecke, "Least-squares orthogonal distances fitting of circle, sphere, ellipse, hyperbola, and parabola", *Pattern Recognition*, Vol. 34, No. 12, 2001, pp. 2283–2303.

[18] Paul Rosin, "Analysing error of fit functions for ellipses", *Pattern Recognition Letters*, Vol. 17, No. 14, 1996, pp. 1461-1470.